IRIS AperTO

UNIVERSITÀ DEGLI STUDI DI TORINO

AperTO - Archivio Istituzionale Open Access dell'Università di Torino

Thermodynamic properties of atrial fibrillation cryoablation: A model-based approach to improve knowledge on energy delivery

This is the author's manuscript

Original Citation:

Availability:

This version is available http://hdl.handle.net/2318/1716081 since 2019-11-19T12:46:52Z

Published version:

DOI:10.1098/rsif.2019.0318

Terms of use:

Open Access

Anyone can freely access the full text of works made available as "Open Access". Works made available under a Creative Commons license can be used according to the terms and conditions of said license. Use of all other works requires consent of the right holder (author or publisher) if not exempted from copyright protection by the applicable law.

(Article begins on next page)

06 December 2021

Thermodynamic properties of atrial fibrillation cryoablation: a model-based approach to improve knowledge on energy delivery

Valter Giaretto[1], Andrea Ballatore[2], Claudio Passerone[3], Paolo Desalvo[2], Mario Matta[2], Andrea Saglietto[2], Mario De Salve[1], Fiorenzo Gaita[4], Bruno Panella[1], Matteo Anselmino[2*]

1 Department of Energy, Politecnico di Torino, Italy

2 Division of Cardiology, "Città della Salute e della Scienza di Torino" Hospital, Department of Medical Sciences, University of Turin, Italy

3 Department of Electronics and Telecommunications, Politecnico di Torino, Italy

4 Cardiology Department, Clinica Pinna Pintor, Turin, Italy

[*]Corresponding Author:

Email: matteo.anselmino@unito.it

Word count: 6397 words, 6 Figures, 38 References

Abstract word count: 199

Conflicts of interest: none related to the present manuscript

Running title: AF cryoablation: a thermodynamic model

Keywords: Ablation, Atrial fibrillation, Cryoballoon, Cryoenergy, Thermodynamic properties

Abstract

Objective: to describe a suitable model of atrial fibrillation cryoablation thermodynamic properties. Methods: three different thermal loads were applied to a cylindrical copper element simulating the cryoprobe, thermally coupled with a Peltier stack producing the freezing effect, and in contact with a bovine liver sample. Thermal events occurring inside the samples were measured using Mirror Image Technique. Results: heat subtracted flux during ice formation and minimum temperature measured at probe–tissue interface were respectively of 1.33 W/cm^2 and -27.8°C for Sample#0, 1.88 W/cm^2 and -35.6°C for Sample#1 and 1.82 W/cm^2 and 1.44 W/cm^2 before and after the ice trigger, respectively, and -29.3°C for Sample#2. Ice trigger temperature was around -8.5°C for Sample#0 and Sample#2, and -10.4°C for Sample#1. In all the investigated samples ice front penetration was proportional to the square root of time and its velocity depended on the heat flux subtracted. The fraction of the useful energy spent for ice formation was less than 60% for Sample#0, about 80% for Sample#1 and for Sample#2, before the reduction of the removed heat flux. Conclusion: freezing time exceeding a cutoff, according to the heat subtracted flux, does not improve the procedure effectiveness and is detrimental to the surrounding tissues.

Introduction

Atrial fibrillation (AF) is the most common tachyarrhythmia in the general population [1]. In case the arrhythmia is symptomatic despite an adequate rate control therapy, a rhythm control strategy, aimed at restoring and maintaining the sinus rhythm, is recommended. In this perspective, catheter ablation for AF is an efficient and established procedure, generally as second-line approach after failure of antiarrhythmic drugs [2]. The main objective of AF ablation is complete isolation of pulmonary veins (PVs) achievable thanks to different technologies. The most frequently used catheter ablation strategy is based on the use of radiofrequency (RF) to induce point-by-point lesions by heating the tissue and leading cells to necrosis; another option consists in using a cryoballoon catheter to create a circular lesion by freezing the tissue of PVs in a single step mode. Both techniques are equally effective for the treatment of drug refractory paroxysmal AF [3–10]. Since there is currently no evidence to suggest that a rhythm control strategy, compared to a rate control therapy with adequate anticoagulation therapy, can improve hard clinical endpoints [11–14], except in the setting of patients with reduced left ventricle ejection fraction [15], the main purpose of AF ablation is to improve symptoms and quality of life. For this reason, safety, rather than effectiveness, must be the key feature of a suitable technique and of an adequate source of energy. Despite the fact that safety of cryoablation, as well as of RF technique, has been established clinically, thorough knowledge on the biological effect of cryoenergy administration on the left atrium is still far to be complete. Therefore, the assessment of thermal behavior and physical properties affecting ice formation and growth in the biological tissue is a key step, holding the potential to improve the safety of cryoablation.

Aim of the present study is to describe a suitable model of the thermodynamic properties of cryoablation in order to better understand the effects of cryoenergy delivery.

Materials and methods

The present study was performed aiming to replicate cooling properties, dimension and probe-tissue interface extension of the clinically used cryoballoon, based on the information provided by the manufacturer (Arctic Front Advance, Medtronic, USA).

The experimental arrangement has been previously illustrated in details [16]; Fig. 1 illustrates a schematic drawing of the setup. To simulate the cryoprobe interface with the tissue, a 25 mm high cylindrical copper element, with a top circular surface of about 1.77 cm2 (assumed equivalent in size to the portion of a cryoballoon surface in contact with the tissues to be treated), hereinafter referred to as cold finger, makes contact with the material under test arranged inside a transparent measurement vessel of parallelepiped shape (square base of 43 mm on each side, and 30 mm high). The freezing effect is produced by a Peltier stack, one side thermally coupled with the cold finger, the other one cooled by a heat exchanger linked to a cold storage maintained at a low temperature (around -18°C) by a chiller.

In the calibration tests, the cooling capacity at the cold finger surface in contact with the tested material (interface I in Fig. 1) was found in the range $0.8 \div 2.5\ \mathrm{W/cm^2}$, with minimum temperatures of -57°C and -40°C, respectively.

In the experiments no temperature sensors were placed inside the tested material, and some thermal events occurring within it were indirectly measured using

temperature information at the cold finger only. This methodology is called Mirror Image Technique, and the cold finger thermally coupled with the sample assumes the role of both a cooling device and a thermal sensor.

The apparatus setup and the experimental methodology validation using water and agar-gel as reference materials [16] showed some relevant results including:

- the beginning of ice formation can be clearly identified by monitoring the consequent sudden temperature perturbation in the cold probe (analogous thermal effect was found in the literature [17] in the case of clinical use of a cryoballoon probe for PV isolation);
- the time evolution of the ice front inside the tested material, just after the onset, follows the square root of time and shows a penetration deepness proportional to the heat flux removed at the cold interface.

Moreover, the early investigation on the ex vivo bovine liver [18] underlined that the beginning of ice formation and its growth in this tissue match what established in the case of agar-gel. From these bases, to confirm such results, the same experimental approach is here proposed to extend the investigation on the ex vivo bovine liver with other thermal loads and scenarios. More liver samples were assembled according to the previous setting, and a picture of this arrangement is shown in Fig. 2. Each sample to be tested is made up by a cylindrical portion of bovine liver, 32 mm in diameter and a few millimeters thick, assembled at one end of an open cylindrical container with the same internal diameter and made in Plexiglas. Reference circular lines engraved on the external surface of the Plexiglas cylinder at different nominal distances L_{ref} from interface I ($z = 0$) were used to estimate the liver thickness and its planarity, with a confidence of ± 0.5mm.

In order to obtain for the liver layer a boundary suitable for assuming the heat diffusion in an ideally semi-infinite medium, the free portion of the cylindrical

container was filled with a solution in distilled water of 2% by weight of agar, of thickness at least equal to its inner diameter. A sheathed thermocouple was immersed in the agar, and placed in contact with the liver surface in the axial position $z = L$, in correspondence of the liver-agar interface L in Fig. 2.

Tested samples have been prepared with the bovine liver obtained from a local animal processing facility, incidentally of different beasts. For the analysis and the comparison of the thermal events occurring inside them, the previously investigated liver sample [18] of thickness $L_0 = 5.5 \pm 0.5$mm has been used as reference, here identified as Sample #0. Two others liver layers, Sample #1 and Sample #2, were arranged inside devoted Plexiglas cylinders, each one of different thickness, $L_1 = 4.5 \pm 0.5$ mm and $L_2 = 7.0 \pm 0.5$ mm , respectively.

In the experiments, with the samples in the center of the measurement vessel coaxially with the cold finger, starting from thermal equilibrium with room temperature, different thermal loads were applied by feeding the Peltier stack with a suitable set of electrical currents.

The sudden temperature increase occurring at the probe-liver interface allowed identifying the ice trigger time t_0, and the subtracted heat flux $q(\tau)$ versus the relative time $\tau = t - t_0$ was established by means of the measured temperatures inside the cold finger [16].

The ice growth $z_f(\tau)$ inside tested materials was measured as detailed in [16] for water and agar gel, and in [18] in the case of bovine liver, all in agreement with a square root function of the previous defined relative time τ. In fact, the composition of the ice penetration $z_f(\tau)$ with the square root of the relative time $\sqrt{\tau}$ gives the function $z_f(\sqrt{\tau})$, so the ice growth is linear versus $\sqrt{\tau}$ and its variation over a time increment $\Delta\tau$ is given by $\Delta z_f(\sqrt{\tau}) = z_f(\sqrt{\tau + \Delta\tau}) - z_f(\sqrt{\tau})$, or simply

proportional to the square root of the relative time $\Delta z_f(\sqrt{\tau}) = m(\sqrt{\tau + \Delta\tau} - \sqrt{\tau})$, where m represents the slope in a plot versus $\sqrt{\tau}$. At the ice trigger time t_0, the function $z_f(\sqrt{\tau})$ is zero (no ice penetration).

Taking into account the linear relationship between the removed heat flux $q_0(\tau)$ and the ice penetration $z_{f,0}(\tau)$ as resulting from Sample #0 [18], in the case of Sample #1 and Sample #2 the ice increment in the axial direction versus square root of the relative time τ was estimated as

$$\Delta z_f(\sqrt{\tau}) = \left\{\frac{q}{q_0}\right\} \Delta z_{f,0}(\sqrt{\tau}) = \left\{\frac{q}{q_0}\right\} [z_{f,0}(\sqrt{\tau + \Delta\tau}) - z_{f,0}(\sqrt{\tau})], \quad (1)$$

where, q and q_0 are the average heat fluxes removed within the chosen time interval $\Delta\tau$, and the ice penetration becomes

$$z_f(\sqrt{\tau + \Delta\tau}) = z_f(\sqrt{\tau}) + \Delta z_f(\sqrt{\tau}) = z_f(\sqrt{\tau}) + \left\{\frac{q}{q_0}\right\} [z_{f,0}(\sqrt{\tau + \Delta\tau}) - z_{f,0}(\sqrt{\tau})]. \quad (2)$$

Due to the transparency of the agar-gel, the beginning of ice formation at $z = L$ has been suitably monitored, and the reliability of the ice penetration obtained with (1) was verified by the measured arriving time τ_L of the ice front at this axial position.

Furthermore, with the help of the measured temperatures at the interface L, some thermal events occurred inside the liver samples were predicted. In particular, with the ice front penetration calculated by (1), considering the frozen and unfrozen properties of ex vivo liver found in literature [19,20], the fraction f expressing the heat flux $q_i(\tau)$ spent for the ice formation with respect to the whole heat flux $q(\tau)$ subtracted by the cryoprobe was obtained by imposing the energy conservation.

In fact, by using the temperatures $T_I(\tau)$ and $T_L(\tau)$ measured at both liver interfaces I and L, with the adoption of a simply lumped thermal model, in which the average properties (thermal conductivity and volumetric heat capacity) of the whole layer are determined with a linear combination of frozen and unfrozen material portions, the energy fraction f has been calculated as

$f(\tau) = \frac{q_i(\tau)}{q(\tau)} = 1 - \frac{q_c(\tau)+\dot{u}(\tau)}{q(\tau)}$, (3)

At a given relative time τ, $q_c(\tau)$ in (3) represents the axial heat flux due to thermal conduction through the liver thickness L caused by the neighboring medium (the agar in our case), while $\dot{u}(\tau)$ denotes the rate of variation of the internal energy per unit of surface of the liver layer. Such heat flux was supposed proportional to the temperature difference $T_L(\tau) - T_I(\tau)$, while the internal energy was assumed proportional to its average temperature.

Results

Graphs representing measured temperatures T_I and T_L versus time are shown in Figs. 3 and 4. The initial time ($t = 0$) of each test corresponds to the start of cooling once the Peltier stack was fed, and the continuous lines represent Sample #0 and Sample #1, while the dashed one refers to Sample #2.

Different cooling scenarios have been produced in the tested samples. In the case of Sample #0 (the reference one), with the assigned feeding currents, the maximum produced cooling rate was found close to 32 K/min (15 K/min just before the ice trigger), obtaining a quite constant heat flux subtracted during ice formation of about 1.33 W/cm^2 and reaching a minimum temperature of -27.8 °C at the probe-liver interface.

Distinct approaches were adopted for investigating Sample #1 and Sample #2. The former was cooled in order to obtain a lower temperature than that of Sample #0 during ice formation, while the latter was subject to different cooling processes by modifying the feeding currents of the Peltier stack during the test.

For Sample #1, with a fixed set of feeding currents, higher than in Sample #0, a maximum cooling rate of 35 K/min was reached at the beginning of the test (20

K/min just before the ice trigger), getting during freezing a fairly stable subtracted heat flux of 1.88 W/cm^2, with a measured probe-liver minimum temperature of -35.6 °C.

As mentioned, Sample #2 was subjected to a cooling process split in two parts. The same set of feeding currents employed for Sample #1 was adopted at the beginning of the test, obtaining the subtracted heat flux of 1.82 W/cm^2. Just after the ice trigger (about 10 s), the current intensities have been reduced in order to produce a freezing process similar to that found for Sample #0, getting in this case a subtracted heat flux of 1.44 W/cm^2 and a minimum temperature of -29.3 °C.

The magnification in the inset of the diagram of Fig. 3 clearly shows for each sample the ice onset time t_0 (the arrows), and the temperature at which it takes place, around -8.5 °C for Sample #0 and Sample #2, and -10.4 °C for Sample #1. The star marker in this figure, and other proposed figures, identifies in the case of Sample #2 the time at which the change on the feeding currents of the Peltier stack was operated.

Temperature trends at the interface between liver and agar displayed in Fig. 4 depend on the sample thickness, and the thermal events produced at the probe-liver interface are not observable if the liver layer is thick enough. In fact, in the case of Sample #2 (the thicker) no thermal consequences are detectable for the ice forming beginning or for the change on the subtracted heat flux at the interface with the probe. For the two thinner samples, with a small delay due to the heat capacity of the liver layer, the ice trigger at the probe-liver interface is noticeable also at the liver-agar interface by analogous perturbation on the measured temperature trend.

Ice front penetration in axial direction versus the square root of the relative time τ is illustrated in Fig. 5. The growth was obtained with (2), assuming a removed average heat flux of 1.33 W/cm^2 for Sample #0 and 1.88 W/cm^2 for Sample #1.

About Sample #2, the average value of the subtracted heat flux was 1.82 W/cm^2 during the first ten seconds after the ice trigger, followed by a value of 1.44 W/cm^2 until the whole freezing of the liver layer. In this plot, the evident slope modification in ice growth is due to the change in shape of the separation surface between phases, as a result of a physical phenomenon depending on properties of the tested material, and to the shape of the contact surface between cryogenic probe and tissue, as discussed in [16]. From the performed tests on Sample #0, a change in growth was noticed when the ice front penetrates about 2.6 mm inside the liver layer, and the same behavior was imposed for Sample #1 and Sample #2 when the calculated ice front reaches that inner position.

Comparisons between the measured and calculated ice front arriving time at the liver-agar interface L are summarized in Fig. 5, where the continuous lines refer to Samples #0 and #1, and the dashed one is that of Sample #2. The circular markers represent the measured values for the arriving time τ_L at the interface with agar, and the error bars refer to the confidence region of ± 10 s in the ice front identification at that interface, and of ± 0.5 mm in the estimated thickness of the sample. Within such confidence region, the measured and the predicted beginning presence of the ice front at the interface L are in good agreement.

In order to investigate the efficiency of the cooling process and to highlight the possible clinical implications of the study, the fraction f of the useful energy spent for ice formation calculated with (3) is shown in Fig. 6.

For Sample #0, Fig. 6 shows that after 60 second less than 60% of the energy flux induces and sustains the ice formation, which is the clinical objective during AF cryoablation, while the remaining fraction of energy cools the surrounding tissue without forming new ice. This percentage remains stable until about 240 seconds, at which ice formation at the liver-agar interface begins (circular marker). The

average ice drift velocity is maximum (≈ 0.2 mm/s) at $\tau = 0$ ($t = t_0$), but it decreases rapidly to approximately stable values (≈ 0.02 mm/s) in a few seconds (data not shown, see Fig. 8 in [18]). A similar behavior can be noticed for Sample #2 when the ice front approaches the liver-agar interface (circular marker) with a reduced heat flux removed ($q = 1.44\ \mathrm{W/cm^2}$). Whereas, when the ice begins forming in the liver the heat removed is higher ($q = 1.82\ \mathrm{W/cm^2}$ before star marker), the energy fraction f is greater than 80%. This behavior is confirmed by Sample #1, in which a quite constant heat flux of 1.88 W/cm^2 is removed during the ice formation, and the average value of the energy fraction f is close to 80% within the time interval taken to reach the liver-agar interface (circular marker).

Discussion

Several clinical trials (AFFIRM [11,12], RACE [13], CABANA [14]) demonstrated that there are no significant differences between rate and rhythm control with regard to mortality from cardiovascular causes, except than in patients with heart failure (Castle AF trial [15]). Therefore, since a reduction of symptoms and a better quality of life are fundamental objectives, efforts in enhancing ablation procedures should be directed towards improving the safety profile as well as its effectiveness and reducing complications rate of the technique.

Catheter ablation for AF is, in fact, an effective and validated procedure for restoring and maintaining sinus rhythm, whose rationale stems from the description that PVs foci are triggers of AF [21]. Currently, the standard and best-established target of paroxysmal and persistent AF catheter ablation is the complete PVs isolation [2]. Despite the fact that this intervention is widely used and well established, the procedure-related complication rate is not marginal (7.8%) [22].

Different studies [3–8], including the multicenter randomized FIRE AND ICE trial [9], proved that cryoballoon ablation is not inferior to RF in terms of efficacy within patients with drug refractory paroxysmal AF. Nevertheless, there are no uniform recommendations or guidelines regarding optimal dosing for AF cryoablation. First recommendations, based on the dosing indications used in the STOP-AF trial [23], suggested a 4-minute application followed by an empirical bonus freeze after PV isolation. Subsequently it has been demonstrated that shorter freezing time, 3-minute application without bonus freeze, was equally effective [24]. In the last years, on the basis of a tailored medicine approach, similarly to focal cryoablation used for the treatment of other supraventricular tachycardias [25], efforts have been directed towards elaborating new dosing protocols based on objective and quantifiable parameters available during the procedure. In this prospective, several markers of durable PV isolation have been examined: time to PV isolation with a cutoff of 60 seconds [26,27] (used as the guiding parameter of different dosing algorithms tested in prospective studies [28,29]), balloon thaw time [27,30], and cryoballoon temperature of less than -51°C (for acute PV isolation [17]). In fact, as shown in Figs. 3 and 4, in our model the temperature curves of the liver-agar interface reflect, as long as the sample is not too thick (7 ± 0,5 mm of sample #2 in our experiment), the thermal events occurring at the probe-liver interface, suggesting that the temperature of the probe or of the cryoballoon can faithfully reflect the temperature in the sample or in the ablated tissue, respectively. This relation is supported by the observation that the temperature curve of an actual cryoballoon probe [17] is very similar to the curves in Fig. 3 and it presents the sudden temperature increase associated with ice formation onset in the tissue. However, it must be kept in mind that, in vivo, different elements (e.g. the degree of PV occlusion, the catheter position, the PVs blood flow) can influence and

modify the two temperatures and the relation between them [27]. Moreover, as previously demonstrated [16], the contact area between the cryoballoon and the tissue is a crucial element for ice formation, since a high thermal contact resistance hampers the ice growth in the ablated tissues. Despite the fact that AF ablation is not an essential intervention quoad vitam, the major efforts have been directed towards identifying markers to improve the procedure and not predictors of complications, which have been studied and are managed especially clinically. Indeed, alongside these studies on possible indicators of an effective ablation, evidences on intraprocedural markers of collateral damage to neighboring structures are still lacking.

The complication rates of AF ablation, both cryoballoon and RF techniques, have been decreased over years [31], due to increased operator experience and technological improvement. However, cryoablation may present complications specific to this ablation strategy and energy source: right phrenic nerve palsy, the most common complication, lesions to esophageal mucosa or formation of atrio-esophageal fistula, and bronchial injury (possibly the underlying mechanism of hemoptysis and cough occurring after the procedure [32,33]). These complications affect structures close to the ablation targets, since a crucial element in their formation is an extreme cooling of the neighboring tissues due to an excessive cryoenergy delivery; therefore, it is fundamental to investigate cryodynamic of the procedure and the behavior of the cooling process.

Although the complications are well managed clinically, increased knowledge on the effects of the cooling process and induction of ice formation in the biological tissues is needed. No quantifiable and biophysical predictors of complications during the ablation procedure have been established, and side effects may manifest after the end of the procedure. Therefore, mainly the patient’s personal risk factors

(age [34,35], anatomical proximity of superior cava vein to right superior PV [36], right PVs proximity to phrenic nerve course and of the left atrium's posterior wall to the esophagus [35,37,38]) and the physician's experience allow the evaluation of the probability of complication manifestation.

Our group has previously demonstrated [16] that in distilled water and agar-gel the liquid-solid transition takes place at a temperature below zero, and that the progression of ice front penetration and the ice volume are proportional to the square root of time and the specific heat removed respectively. These results, except for the ice volume-specific heat removed relation, that has not been investigated, have been confirmed in the present experimental arrangement consisting of a bovine liver sample (Fig. 3, Fig. 5). The present work aims at analyzing, with a model-based approach, the thermodynamic properties of cryoablation in a biological tissue. As regard to the ice trigger temperature there is not a unique reason to explain the observed discrepancy among the samples in Fig. 3. Probably it is due to minimal differences of the thermal contact with the liver sample or to the different amount of liquid phase at the probe-liver interface. In fact, previous experiments on water and agar-gel [16] had shown the effect of the thermal contact resistance between probe and tested materials, reducing such temperature in agreement to its magnitude, and in absence of that resistance ice forming temperatures of -7.0 °C and -12.4 °C, for case of agar and water respectively, were found.

The fraction of the useful energy for ice formation as a function of relative time shown in Fig. 6 and the average ice drift velocity curve of Sample #0 (Fig. 8 in [18]) demonstrate that ice formation rate within the tissue is already reduced after a few seconds. Since the ice formation is a crucial element for cellular death, this finding is fundamental to understand the biology of the cooling process and it

supports the clinically established indication to reduce freezing time of the procedure. Interestingly, Fig. 6 shows that by increasing the subtracted heat flux, which, from a clinical point of view, is achieved by improving the contact between the cryoballoon and the PV and is reflected, for example, in a lower minimum temperature, the efficiency of the freezing phenomenon is improved (i.e. a greater fraction of energy is transformed to utile work and not to collateral unwanted cooling of surrounding tissues). Indeed, since the ice forming fraction of energy in Sample #1 is greater than that in Sample #0 (about 75% and 55% at 60 seconds, respectively, according to our model), there is an improved control of cryoenergy delivery and a lower cooling of the surrounding tissue. This observation is of the utmost importance since it demonstrates that a low subtracted heat flux subsequent to a poor cryoballoon-PV contact cannot be simply offset by a longer freezing ablation time, as, although procedure effectiveness, resulting from transmural ice formation, may be the same, damage to surrounding tissue would be greater. A better understanding of the thermal diffusion laws has, in fact, the potential to suggest a procedural cooling protocol, to date not based on thermodynamic data, predicting the ideal heat flux achieving the desired effect by limiting to the minimum unwanted cooling of surrounding tissues. According to Fig. 5 and based on the temperature curve shown in Fig. 3, it takes about two and a half minutes for the front of the ice in Sample #0 to reach 4 mm (representative of the outer edge of the cardiac tissue considering the average atrial thickness), about eighty seconds in Sample #1 and about two minutes in Sample #2. Since there are differences in the cooling/heating dynamics between the experimental arrangement and the original cryoballoon, these values cannot be intended as cutoffs to be used in a clinical scenario, but they clearly indicate that variations in values of the subtracted heat flux deeply affect the velocity of ice penetration, and consequently the optimal

ablation duration. Moreover, since the ice front penetration is proportional to the square root of time, as the ablation proceeds, a longer freezing time corresponds to a lower advancement of the ice and, since the ice forming percentage of thermal energy flux decreases, to a greater, unneeded cooling of the surrounding tissues. Therefore, as time progresses, there is a little advance in ice penetration, at the expense of a large cooling of the adjacent tissues, which has been demonstrated to be an important mechanism of complications development. The demonstration of the hypothesis that the cooling process is a thermal diffusion process was a crucial aspect of this work. The fact that the formulated thermal diffusion equation reflects faithfully what was observed and measured during the experiment confirmed that the model is reliable and rigorously designed, and allowed to make predictions on the behavior of ice front penetration in a biological tissue. On these bases, it is possible to study different cooling scenarios being confident that the results are in keeping with reality. Moreover, it will allow to study and evaluate cooling protocols different to those actually in use in clinical practice in order to analyze the thermal behavior of the tissue and to assess the effects and possible advantages of these protocols. Finally, according to the fact that an increase in the subtracted heat flux corresponds to a faster ice penetration and a greater ice forming percentage of thermal energy flux, it must be kept in mind that a cryoablation duration prolonged beyond what is necessary results in a greater damage to surrounding tissues especially if the subtracted heat flux is high. Indeed, bearing in mind that a high subtracted heat flux leads to a greater efficiency, as shown in Fig. 6, an excessive freezing ablation time with the cryoballoon well positioned and perfectly in contact with the PV antrum causes greater damage to surrounding tissues, since, once transmural ice has formed, ice formation progresses more quickly. Hence the demonstration, on a non-clinical basis, of the need to shorten ablation times if the

intra-procedural cryodynamic parameters are good. These data bring new important elements in favor of this indication, since in clinical experience it is not common practice and ablation duration for each PV is often standard 4 minutes.

Limitations

This study presents some limitations. First, the experimental setting, although using largely validated models and phantoms mimicking the human tissues properties, is not so accurate to directly transpose the results to the clinical setting. Some differences directly stem from the necessary ex-vivo experimental arrangement. In particular, the absence of blood flow modelling, along with the potential implications of cellular metabolism, different patients' body temperature and different thickness of the atrial wall from patient to patient, are all variables that impact on the cooling dynamics properties of the probe-tissue interface. Although similar, since both physiologically composed by a homogenous parenchyma of mostly a single component of cells and a modest portion of adipose tissue, another limitation relates to differences between hepatic and cardiac tissues. However, the aim of this work is to evaluate from a thermodynamic point of view the cooling process and study thermal diffusion in a biological tissue, and not in a homogenous artificial material, in order to describe general laws of the thermal behavior. These laws, assessed in a liver sample, would perhaps require correction factors to be applicable to the heart, however the general considerations arising from this work would stay valid. Finally, the cryoprobe model used in this experiment, despite its modelling meant to replicate as closely as possible cryoballoon features, in order to minimize this bias, is different from the original cryoballoon. The major evident discrepancy is the cooling/heating dynamics, because the heat capacity of the cold

finger makes obtaining high temperature rates at the probe outer boundary arduous. With the arranged apparatus, the time interval required to reach a minimum stable temperature is longer than that expected for the clinical cryoprobe.

Conclusions

The present work describes a reliable model to study thermodynamic properties of cryoballoon ablation and predict thermal behavior of a biological tissue subjected to freezing, paving the way for further analysis on differentiated cooling protocols. Indications to shorten ablation time are mostly driven by clinical studies aimed mainly at assessing and improving the effectiveness of the procedure, whereas evidences on the biological effect and the thermal events induced by cryoablation are poor. This model sheds some light on this aspect of cryoablation, clarifying some unclear elements and providing new insights, aiming to improve procedure's safety: the efficiency of the ablation changes with the variations in subtracted heat flux; and a longer ablation with poor balloon-PV contact is different to a shorter ablation with optimal balloon-PV contact, with regard to the effects on surrounding tissues. Finally, the present model provides additional information for an effective and safe cryoballoon ablation, suggesting that freezing time above a certain cutoff, that varies according to the heat subtracted flux, is not useful to improve the procedure effectiveness and may be detrimental to surrounding tissues.

Acknowledgments

This study was performed thanks to the support of the Italian Ministry of Health "Ministero della Salute" within the project "Bando Finalizzata 2016: Sezione GR,

Change promoting: Cryoballoon atrial fibrillation ablation: in vivo evaluation of tissue effects and predictors of durable lesions (GR-2016-02362088)", and of the Energy Dept. of the Politecnico di Torino within the BioTherm project 2017 involving "Transport properties of biological systems". Funded authors: Dr. Matteo Anselmino and Prof. Valter Giaretto, respectively. The funders had no role in study design, data collection and analysis, decision to publish, or preparation of the manuscript

References

1. Andrade J, Khairy P, Dobrev D, Nattel S. 2014 The clinical profile and pathophysiology of atrial fibrillation: Relationships among clinical features, epidemiology, and mechanisms. *Circ. Res.* (doi:10.1161/CIRCRESAHA.114.303211)
2. Kirchhof P *et al.* 2016 2016 ESC Guidelines for the management of atrial fibrillation developed in collaboration with EACTS. *Eur. J. Cardiothorac. Surg.* (doi:10.1093/ejcts/ezw313)
3. Luik A *et al.* 2015 Cryoballoon Versus Open Irrigated Radiofrequency Ablation in Patients With Paroxysmal Atrial Fibrillation. *Circulation* **132**, 1311–1319. (doi:10.1161/CIRCULATIONAHA.115.016871)
4. Wasserlauf J *et al.* 2015 Cryoballoon versus radiofrequency catheter ablation for paroxysmal atrial fibrillation. *PACE - Pacing Clin. Electrophysiol.* (doi:10.1111/pace.12582)
5. Aryana A *et al.* 2015 Acute and long-term outcomes of catheter ablation of atrial fibrillation using the second-generation cryoballoon versus open-irrigated radiofrequency: A multicenter experience. *J. Cardiovasc. Electrophysiol.* (doi:10.1111/jce.12695)
6. Hunter RJ *et al.* 2015 Point-by-Point Radiofrequency Ablation Versus the Cryoballoon or a Novel Combined Approach: A Randomized Trial Comparing 3 Methods of Pulmonary Vein Isolation for Paroxysmal Atrial Fibrillation (The Cryo Versus RF Trial). *J. Cardiovasc. Electrophysiol.* (doi:10.1111/jce.12846)
7. Jourda F *et al.* 2014 Contact-force guided radiofrequency vs. second-generation balloon cryotherapy for pulmonary vein isolation in patients with paroxysmal atrial fibrillation - A prospective evaluation. *Europace* (doi:10.1093/europace/euu215)
8. Squara F *et al.* 2015 Comparison between radiofrequency with contact force-sensing and second-generation cryoballoon for paroxysmal atrial fibrillation catheter ablation: A multicentre European evaluation. *Europace* (doi:10.1093/europace/euv060)

9. Kuck K-H *et al.* 2016 Cryoballoon or Radiofrequency Ablation for Paroxysmal Atrial Fibrillation. *N. Engl. J. Med.* **374**, 2235–2245. (doi:10.1056/NEJMoa1602014)
10. Matta M, Anselmino M, Ferraris F, Scaglione M, Gaita F. 2018 Cryoballoon vs. radiofrequency contact force ablation for paroxysmal atrial fibrillation: A propensity score analysis. *J. Cardiovasc. Med.* (doi:10.2459/JCM.0000000000000633)
11. Greene HL. 2002 Baseline characteristics of patients with atrial fibrillation: The AFFIRM study. *Am. Heart J.* **143**, 991–1001. (doi:10.1067/mhj.2002.122875)
12. Investigators TAFFI of RM (AFFIRM). 2002 A Comparison of Rate Control and Rhythm Control in Patients with Atrial Fibrillation. *N. Engl. J. Med.* **347**, 1825–1833. (doi:10.1056/NEJMoa021328)
13. Van Gelder IC *et al.* 2002 A Comparison of Rate Control and Rhythm Control in Patients with Recurrent Persistent Atrial Fibrillation. *N. Engl. J. Med.* **347**, 1834–1840. (doi:10.1056/NEJMoa021375)
14. Packer DL *et al.* 2019 Effect of Catheter Ablation vs Antiarrhythmic Drug Therapy on Mortality, Stroke, Bleeding, and Cardiac Arrest Among Patients With Atrial Fibrillation. *JAMA* **55902**. (doi:10.1001/jama.2019.0693)
15. Marrouche NF *et al.* 2018 Catheter Ablation for Atrial Fibrillation with Heart Failure. *N. Engl. J. Med.* **378**, 417–427. (doi:10.1056/NEJMoa1707855)
16. Giaretto V, Passerone C. 2017 Mirror image technique for the thermal analysis in cryoablation: Experimental setup and validation. *Cryobiology* **79**, 56–64. (doi:10.1016/j.cryobiol.2017.09.001)
17. Fürnkranz A, Köster I, Chun KRJ, Metzner A, Mathew S, Konstantinidou M, Ouyang F, Kuck KH. 2011 Cryoballoon temperature predicts acute pulmonary vein isolation. *Heart Rhythm* **8**, 821–825. (doi:10.1016/j.hrthm.2011.01.044)
18. Giaretto V, Passerone C. 2018 Experimental Investigation on the Ice Formation and Growth in Ex Vivo Bovine Liver. *Am. J. Biosci.* **6**, 35–44. (doi:10.11648/j.ajbio.20180603.11)

19. Cheolkyun Kim, O'Rourke AP, Will JA, Mahvi DM, Webster JG. 2008 Finite-Element Analysis of Hepatic Cryoablation Around a Large Blood Vessel. *IEEE Trans. Biomed. Eng.* **55**, 2087–2093. (doi:10.1109/TBME.2008.919837)

20. Chan JY, Ooi EH. 2016 Sensitivity of thermophysiological models of cryoablation to the thermal and biophysical properties of tissues. *Cryobiology* **73**, 304–315. (doi:10.1016/j.cryobiol.2016.10.006)

21. Haïssaguerre M *et al.* 1998 Spontaneous Initiation of Atrial Fibrillation by Ectopic Beats Originating in the Pulmonary Veins. *N. Engl. J. Med.* **339**, 659–666. (doi:10.1056/NEJM199809033391003)

22. Arbelo E *et al.* 2017 Contemporary management of patients undergoing atrial fibrillation ablation: in-hospital and 1-year follow-up findings from the ESC-EHRA atrial fibrillation ablation long-term registry. *Eur. Heart J.* **38**, ehw564. (doi:10.1093/eurheartj/ehw564)

23. Packer DL *et al.* 2013 Cryoballoon Ablation of Pulmonary Veins for Paroxysmal Atrial Fibrillation. *J. Am. Coll. Cardiol.* **61**, 1713–1723. (doi:10.1016/j.jacc.2012.11.064)

24. Ciconte G *et al.* 2015 Single 3-minute freeze for second-generation cryoballoon ablation: One-year follow-up after pulmonary vein isolation. *Heart Rhythm* **12**, 673–680. (doi:10.1016/j.hrthm.2014.12.026)

25. Matta M, Anselmino M, Scaglione M, Vitolo M, Ferraris F, Di Donna P, Caponi D, Castagno D, Gaita F. 2017 Cooling dynamics: a new predictor of long-term efficacy of atrioventricular nodal reentrant tachycardia cryoablation. *J. Interv. Card. Electrophysiol.* **48**, 333–341. (doi:10.1007/s10840-016-0208-4)

26. Ciconte G *et al.* 2015 On the Quest for the Best Freeze. *Circ. Arrhythmia Electrophysiol.* **8**, 1359–1365. (doi:10.1161/CIRCEP.115.002966)

27. Aryana A *et al.* 2016 Procedural and biophysical indicators of durable pulmonary vein isolation during cryoballoon ablation of atrial fibrillation. *Heart Rhythm* **13**, 424–432. (doi:10.1016/j.hrthm.2015.10.033)

28. Aryana A, Kenigsberg DN, Kowalski M, Koo CH, Lim HW, O'Neill PG, Bowers MR, Hokanson RB, Ellenbogen KA. 2017 Verification of a novel atrial fibrillation cryoablation dosing algorithm guided by time-to-pulmonary vein isolation: Results from the Cryo-DOSING Study (Cryoballoon-ablation DOSING Based on the Assessment of Time-to-Effect and Pulmonary Vein Isolation Gu. *Heart Rhythm* **14**, 1319–1325. (doi:10.1016/j.hrthm.2017.06.020)

29. Chun KRJ, Stich M, Fürnkranz A, Bordignon S, Perrotta L, Dugo D, Bologna F, Schmidt B. 2017 Individualized cryoballoon energy pulmonary vein isolation guided by real-time pulmonary vein recordings, the randomized ICE-T trial. *Heart Rhythm* **14**, 495–500. (doi:10.1016/j.hrthm.2016.12.014)

30. Ghosh J, Martin A, Keech AC, Chan KH, Gomes S, Singarayar S, McGuire MA. 2013 Balloon warming time is the strongest predictor of late pulmonary vein electrical reconnection following cryoballoon ablation for atrial fibrillation. *Heart Rhythm* **10**, 1311–1317. (doi:10.1016/j.hrthm.2013.06.014)

31. Muthalaly RG *et al.* 2018 Temporal trends in safety and complication rates of catheter ablation for atrial fibrillation. *J. Cardiovasc. Electrophysiol.* **29**, 854–860. (doi:10.1111/jce.13484)

32. ARYANA A, BOWERS MR, HAYATDAVOUDI SM, ZHANG Y, AFIFY A, D'AVILA A, O'NEILL PG. 2016 Impact of Pulmonary Vein Cryoballoon Ablation on Bronchial Injury. *J. Cardiovasc. Electrophysiol.* **27**, 861–867. (doi:10.1111/jce.12983)

33. BHAGWANDIEN R, VAN BELLE Y, DE GROOT N, JORDAENS L. 2011 Hemoptysis After Pulmonary Vein Isolation with a Cryoballoon: An Analysis of the Potential Etiology. *J. Cardiovasc. Electrophysiol.* **22**, 1067–1069. (doi:10.1111/j.1540-8167.2011.02031.x)

34. Guhl EN *et al.* 2016 Incidence and Predictors of Complications During Cryoballoon Pulmonary Vein Isolation for Atrial Fibrillation. *J. Am. Heart Assoc.* **5**, 1–7. (doi:10.1161/JAHA.116.003724)

35. Matsumoto Y *et al.* 2019 Predicting factors of transmural thermal injury after cryoballoon pulmonary vein isolation. *J. Interv. Card. Electrophysiol.* **54**, 101–108. (doi:10.1007/s10840-018-0454-8)

36. Kühne M, Knecht S, Altmann D, Kawel N, Ammann P, Schaer B, Osswald S, Sticherling C. 2013 Phrenic nerve palsy during ablation of atrial fibrillation using a 28-mm cryoballoon catheter: predictors and prevention. *J. Interv. Card. Electrophysiol.* **36**, 47–54. (doi:10.1007/s10840-012-9740-z)

37. Ströker E *et al.* 2016 Anatomic predictors of phrenic nerve injury in the setting of pulmonary vein isolation using the 28-mm second-generation cryoballoon. *Heart Rhythm* **13**, 342–351. (doi:10.1016/j.hrthm.2015.10.017)

38. Ang R *et al.* 2015 Pulmonary vein measurements on pre-procedural CT/MR imaging can predict difficult pulmonary vein isolation and phrenic nerve injury during cryoballoon ablation for paroxysmal atrial fibrillation. *Int. J. Cardiol.* **195**, 253–258. (doi:10.1016/j.ijcard.2015.05.089)

Figures

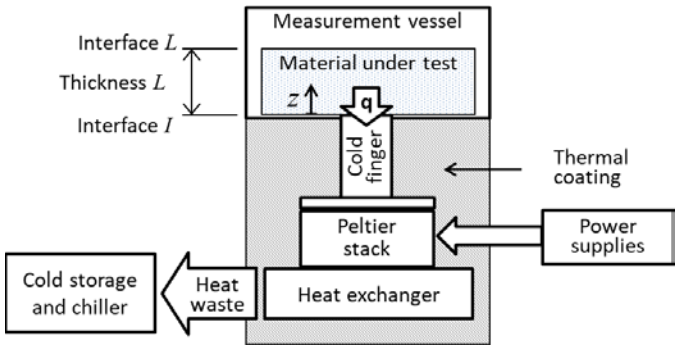

Fig. 1. Experimental apparatus schematic representation.

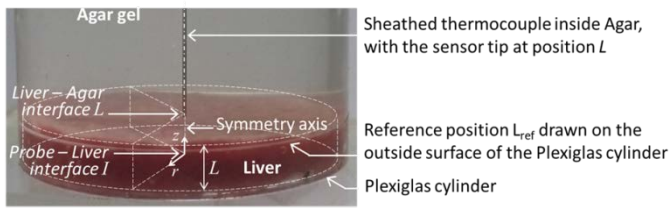

Fig. 2. Arrangement of the liver sample, and the geometric reference; materials and their interfaces are also shown.

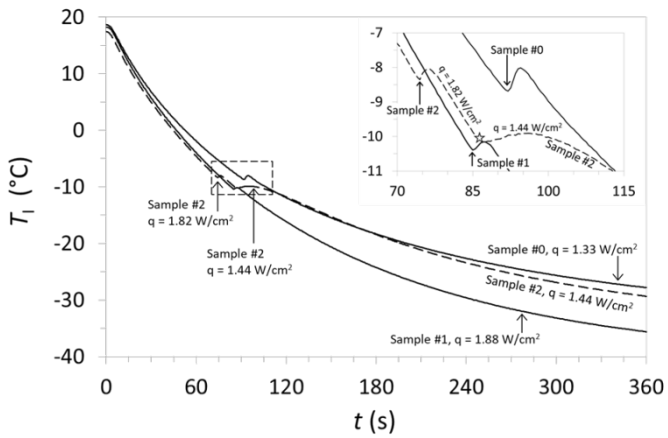

Fig.3. Evolution in time of temperatures at the probe–liver interface for the three samples. Inset: magnification of the graphs at the ice triggering instant

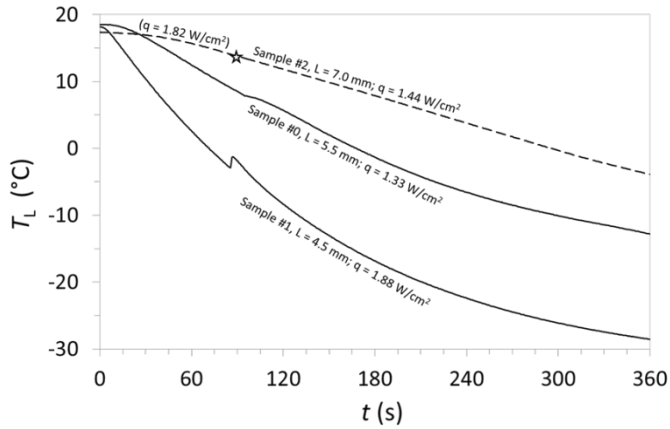

Fig. 4. Evolution in time of temperatures at the liver–agar interface for the three samples

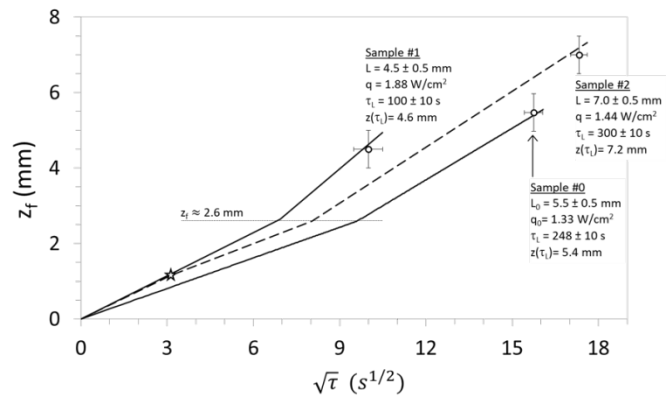

Fig. 5. Estimated ice front penetration versus the square root of relative time $\tau = t - t_0$. Circular markers with error bars represent the ice detected at the liver-agar interface

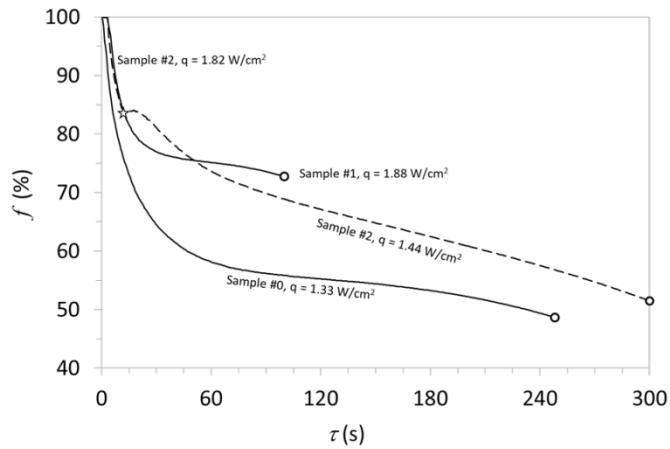

Fig. 6. Fraction f of the useful energy for ice formation as a function of relative time $\tau = t - t_0$.